Journal of Solid State Chemistry **161,** 38–44 (2001)
doi:10.1006/jssc.2001.9264, available online at http://www.idealibrary.com on IDEAL®

The Reduction of Mg–Fe–O and Mg–Fe–Al–O Complex Oxides Studied by Temperature-Programmed Reduction Combined with *in Situ* Mössbauer Spectroscopy

Xin Ge, Mingshi Li, and Jianyi Shen[1]

Department of Chemistry, Nanjing University, Nanjing, 210093 China

Received January 4, 2001; in revised form May 16, 2001; accepted June 7, 2001; published online August 22, 2001

In a H_2/N_2 atmosphere, the reduction processes of Mg–Fe–O and Mg–Fe–Al–O complex oxide catalysts, derived from their hydrotalcite precursors, were studied by means of temperature-programmed reduction (TPR). In particular, the reduction process of the Mg–Fe–O samples with a Mg/Fe ratio of 1/1 and Mg–Fe–Al–O with a Mg/Fe/Al ratio of 2/1/1 were investigated in detail in combination with *in situ* Mössbauer spectroscopy and X-ray diffraction (XRD). For the Mg–Fe–O sample, two peaks were observed in the TPR profile with peak temperatures at 446 and 696°C, respectively, indicating that the reduction of the oxide catalyst proceeded via two stages. Mössbauer spectroscopy and XRD showed that the phases in the sample were $MgFe_2O_4$ and MgO before TPR. At the first TPR peak (446°C), $MgFe_2O_4$ was completely reduced to $Mg_{1-x}Fe_xO$. The Mössbauer spectrum of $Mg_{1-x}Fe_xO$ exhibited a doublet with IS = 0.83 mm/s and QS = 0.87 mm/s. The second TPR peak (696°C) corresponded to the reduction of $Mg_{1-x}Fe_xO$ to Fe^0. For the Mg–Fe–Al–O sample, two peaks were also observed in the TPR profile with temperatures at 506 and 936°C, respectively. Mössbauer spectroscopy and XRD showed that the phases in the sample were α-Fe_2O_3, $MgFeAlO_4$, and MgO before TPR. The Mössbauer spectrum of $MgFeAlO_4$ was a doublet with IS = 0.33 mm/s and QS = 0.76 mm/s. At the first TPR peak (506°C), α-Fe_2O_3 was reduced to Fe^{2+} and Fe^0, while $MgFeAlO_4$ was transformed into $Mg_{1-x}Fe_xO$. The second TPR peak (936°C) corresponded to the reduction of $Mg_{1-x}Fe_xO$ to metallic Fe^0. Effects of the presence of magnesium and aluminum in the solid solutions on the reduction of iron species were discussed. © 2001 Academic Press

Key Words: **temperature-programmed reduction; Mössbauer spectroscopy; Mg–Fe–O binary complex oxide; Mg–Fe–Al–O trinary complex oxide; oxide–oxide interaction.**

INTRODUCTION

Iron-based catalytic materials are commonly used in ammonia and Fischer–Tropsch synthesis. Promoters are usually used for the bulk and supported catalysts. The advantage of using magnesia as the support is that it can also act as a promoter (1–6). The Mg–Fe–O catalyst resulting from the reduction of hydrotalcite precursors exhibited much higher olefin selectivity in the Fischer–Tropsch synthesis than the pure iron catalyst reduced from Fe_2O_3 (6). The high olefin selectivity might result from the basicity of MgO. Alumina is widely used as a catalyst support. The important feature of γ-alumina is its stability of surface area. Thus, alumina is often used as a structure promoter. However, the interactions among iron, magnesium, and aluminum in solid solutions are complicated (1–3, 7–10). In the present work, the effects of Mg and Al on the reduction of iron in the Mg–Fe–O and Mg–Fe–Al–O solid solutions are studied to probe such interactions.

Temperature-programmed reduction (TPR) is a thermal method that can be used for the analysis of the reduction of metal oxides. In fact, the technique has been applied for the study of catalytic materials and their preparation procedures (11–13). Typically, a sample is subjected to a predetermined linear heating rate and reduction of the sample is monitored by measuring the consumption of H_2. The resulting TPR profile contains information on the nature of the reducible species present in the sample. For example, it can provide information about the dispersion of supported components as well as the metal oxide–support and oxide–oxide interactions in catalysts. However, the reduction steps are sometimes so complicated that the reduction peaks in a TPR profile are not easily explained. In this regard, Mössbauer spectroscopy becomes a powerful technique that can be used for the determination of chemical states of some elements after each TPR peak (14, 15). Recently, we used the *in situ* TPR-Mössbauer technique and studied some iron-containing catalytic materials (16–21). The same technique was used to study the reduction processes of MgO–Fe–O and Mg–Fe–Al–O complex metal oxides in this work. In addition, X-ray diffraction (XRD) was used besides the Mössbauer spectroscopy to

[1] To whom correspondence should be addressed. Fax: 86-25-3317761. E-mail: jyshen@nju.edu.cn

0022-4596/01 $35.00

confirm the phases in the samples at different reduction stages.

EXPERIMENTAL

Hydrotalcite-like compounds with Mg/Fe/Al ratios of 1/1/0, 4/3/1, 2/1/1, and 4/1/3 were prepared by the co-precipitation method (6). Specifically, $Mg(NO_3)_2 \cdot 6H_2O$ (AR), $Fe(NO_3)_3 \cdot 9H_2O$ (AR), and $Al(NO_3)_3 \cdot 9H_2O$ (AR) with desired ratios were mixed to obtain 230 ml of aqueous solution with the total cation concentration of 1 mol/dm^3. NH_4OH (AR) and $(NH_4)_2CO_3$ (AR) were dissolved in deionized water to form another aqueous solution of 350 ml with appropriate amounts calculated according to the relations of $[NH_4OH] = 2.2[Mg^{2+}] + 3.2([Fe^{3+}] + [Al^{3+}])$, and $[CO_3^{2-}] = 0.5([Fe^{3+}] + [Al^{3+}])$. Then, the two solutions were added dropwise into 250 ml of deionized water at 40°C in a 1000-ml beaker over an interval of 30 min, during which time a brown precipitate was formed. The pH of the slurry was controlled in the range of 8 to 9 by adding the two solutions alternately. After the two solutions were completely added, the precipitate formed was filtered, washed with deionized water, and dried at 120°C. The samples were calcined at 400°C for 4 h. The specific surface areas of the calcined samples with Mg/Fe/Al ratios of 1/1/0, 4/3/1, 2/1/1, and 4/1/3 were measured to be 69, 82, 82, and 80 m^2/g, respectively.

The TPR apparatus used in this work is similar to that described elsewhere (22). About 20 mg of sample was loaded in a quartz U-tube. A mixture of N_2 and H_2 (5% H_2) with purity of 99.999% was used, and the flow rate was maintained at 20 ml/min. The temperature was raised at a programmed rate of 10°C/min from room temperature to around 1200°C. The amount of hydrogen consumed for each peak in the TPR profile was obtained from the peak area with a normalization method.

To collect Mössbauer spectra without exposing the sample to air after each TPR peak, an *in situ* quartz cell was adopted as described elsewhere (15). About 100 mg of the sample was used to obtain good Mössbauer spectra. For each TPR peak, the temperature was raised to the peak position and then maintained until the peak was complete. The sample was then cooled down to room temperature in flowing H_2/N_2 and sealed for a Mössbauer measurement. The Mössbauer spectra were recorded using a 15 mC$_i$ ^{57}Co(Pd) source on a constant acceleration spectrometer. The spectra were computer-fitted to the Lorentzian lines by a least-squares program. The velocity of the spectrometer was calibrated with respect to α-Fe.

XRD measurements were performed in an ambient atmosphere after the collection of Mössbauer spectra using the Rigaku D/Max-RA X-ray diffractometer equipped with a Cu target and graphite monochromator. The voltage and current employed were 40 kV and 120 mA, respectively.

RESULTS AND DISCUSSION

1. *The Temperature-Programmed Reduction Profiles of Mg–Fe–O and Mg–Fe–Al–O Complex Oxides*

Two main reduction peaks at 380 and 684°C in the TPR profile of a α-Fe_2O_3 sample were observed (17). The two TPR peaks corresponded to the hydrogen consumption of 11.2 and 88.8%. The area ratio is approximately 1:8, which can be attributed to the two sequential reductions

$$3Fe_2O_3 + H_2 = 2Fe_3O_4 + H_2O \quad [1]$$

$$2Fe_3O_4 + 8H_2 = 6Fe + 8H_2O. \quad [2]$$

Thus, the reduction of Fe_2O_3 proceeds via two steps from Fe_2O_3 to Fe_3O_4 and then to Fe. Bulk-phase wustite (FeO) is thermodynamically metastable and can hardly be detected during the reduction of Fe_2O_3 to Fe (23, 24).

As shown in Fig. 1a, the Mg–Fe–O complex oxide with the Mg/Fe atomic ratio of 1/1 exhibited the TPR profile

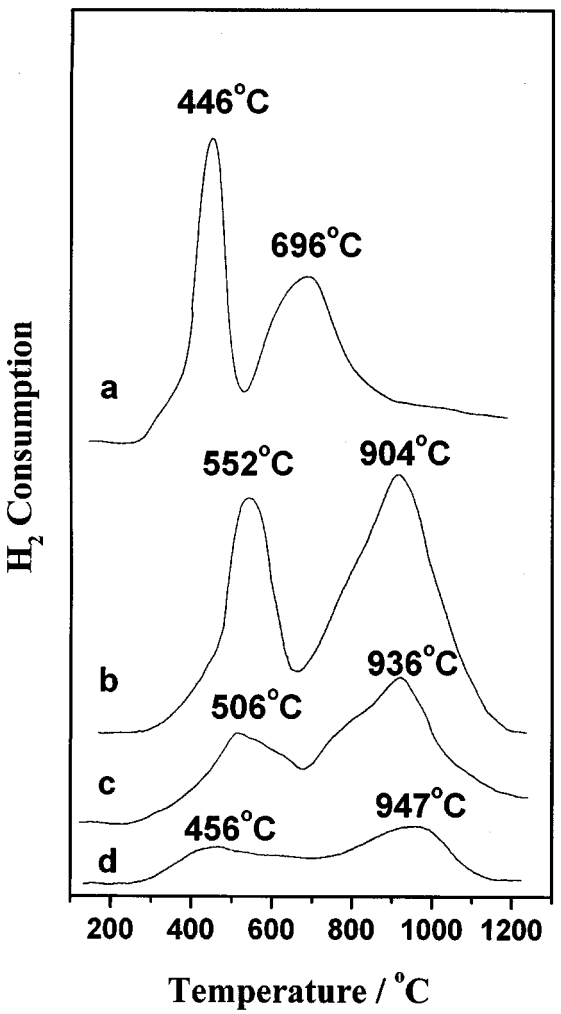

FIG. 1. TPR profiles of Mg–Fe–O and Mg–Fe–Al–O samples with different Mg/Fe/Al atomic ratios: (a) 1/1/0, (b) 4/3/1, (c) 2/1/1, and (d) 4/1/3.

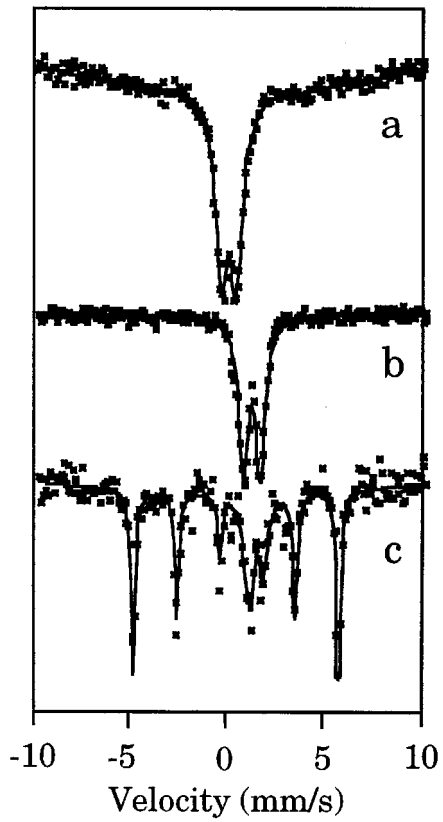

FIG. 2. *In situ* Mössbauer spectra for the Mg–Fe–O sample with the Mg/Fe ratio of 1/1 collected (a) before the reduction, (b) after the first TPR peak, and (c) after the second TPR peak.

with two peaks around 446 and 696°C, respectively, which are significantly higher than those for pure α-Fe_2O_3. The ratio of the two peaks is about 1:1, indicating the different reduction process for the Mg–Fe–O sample as compared to that of the pure α-Fe_2O_3. Upon the addition of Al, the resulted Mg–Fe–Al–O samples exhibited even higher peak temperatures, indicating the stronger interactions among different components. For example, the Mg–Fe–Al–O sample with the Mg/Fe/Al ratio of 4/3/1 displayed the two TPR peaks at 522 and 904°C, respectively. To understand these interactions, it should be desirable to understand what has happened during the TPR. Thus, the Mg–Fe–O sample and the Mg–Fe–Al–O with the Mg/Fe/Al atomic ratio of 2/1/1 were further examined in detail with *in situ* Mössbauer spectra and XRD after each TPR peak.

2. *The Reduction Process of Mg–Fe–O Binary Oxide*

Figures 2 and 3 show the Mössbauer spectra and XRD patterns, respectively, collected for the Mg–Fe–O sample after calcination and after each TPR peak as represented in Fig. 1a. The Mössbauer parameters and assignments of corresponding iron species and the different phases detected by XRD are given in Table 1.

As shown in Fig. 2a, the Mg–Fe–O sample before the reduction displayed a doublet with the isomer shift (IS) of 0.30 mm/s and quadrupole splitting (QS) of 0.76 mm/s, which is typical of superparamagnetic Fe^{3+} species. This spectrum may be assigned to $MgFe_2O_4$ (1, 6, 25, 26) and was confirmed by XRD (27). In addition, the presence of MgO in the sample was also detected by XRD (28).

After the first TPR peak at 446°C, the reduction of the sample led to the formation of Fe^{2+}, as revealed by the doublet with IS = 0.83 mm/s and QS = 0.87 mm/s in the Mössbauer spectrum shown in Fig. 2b. This doublet can be assigned to $Mg_{1-x}Fe_xO$ according to Connell and Dumesic (26) and Tu *et al.* (29). The XRD pattern shown in Fig. 3b confirmed the formation of $Mg_{1-x}Fe_xO$, which exhibits the

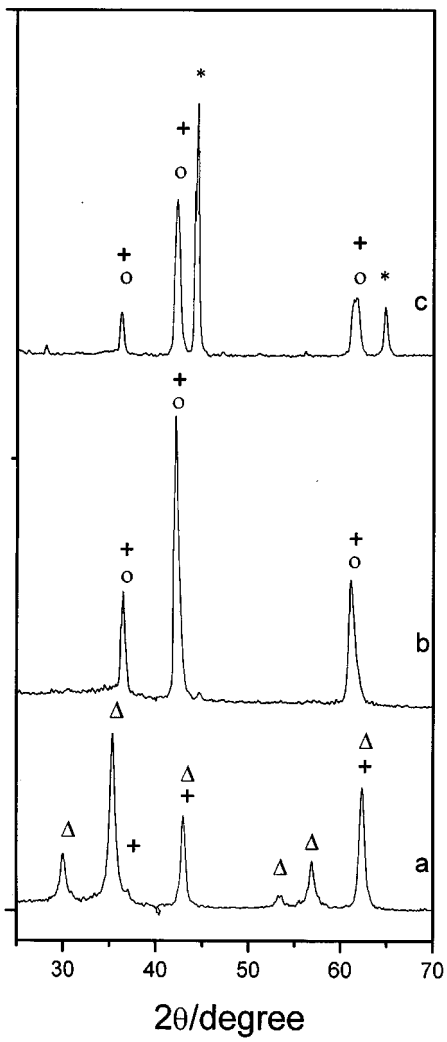

FIG. 3. The XRD patterns for the Mg–Fe–O sample with the Mg/Fe ratio of 1/1 collected (a) before the reduction, (b) after the first TPR peak, and (c) after the second TPR peak. The symbols for the phases are (△) $MgFe_2O_4$, (+) MgO, (O) $Mg_{1-x}Fe_xO$, and (*) α-Fe.

TABLE 1
Mössbauer Parameters and Assignments of Iron Species and Phases Detected by XRD for the Fe–Mg–O Sample (Mg/Fe = 1/1) before the Reduction and after Each TPR Peak

		Mössbauer results						
Peak in TPR	Peak temperature (°C)	IS ($mm\,s^{-1}$)	QS ($mm\,s^{-1}$)	HF (kOe)	FWHM ($mm\,s^{-1}$)	Relative peak area	Iron species assignment	Phases by XRD
Before reduction		0.30	0.76	—	0.54	100	Fe^{3+}	$MgFe_2O_4$ MgO
First peak	446	0.83	0.87	—	0.57	100	Fe^{2+}	$Mg_{1-x}Fe_xO$ MgO
Second peak	696	0.02	—	327	—	71	Fe^0	Fe
		1.02	0.82	—	0.49	29	Fe^{2+}	$Mg_{1-x}Fe_xO$ MgO

characteristic diffraction peaks at $d = 3.05$, 2.04, and 1.17 (30). However, it should be noted that the MgO displays the exact same peak positions as $Mg_{1-x}Fe_xO$. Thus, the presence of MgO in the sample after the first TPR peak cannot be excluded. Both Mössbauer and XRD demonstrated the disappearance of the $MgFe_2O_4$ phase after the first TPR peak. Therefore, we may describe the process for the first TPR peak at 446°C as the reduction of $MgFe_2O_4$ to $Mg_{1-x}Fe^{II}_xO$:

$$MgFe^{III}_2O_4 + H_2 = Mg_{1-x}Fe^{II}_xO + H_2O. \qquad [3]$$

Figure 2c presents the Mössbauer spectrum collected after the second TPR peak for the Mg–Fe–O sample. This spectrum displays a sextuplet plus a doublet in the center. The sextuplet has the inner hyperfine field of 327 kOe, characteristic of α-Fe. The doublet belongs to the unreduced $Mg_{1-x}Fe_xO$. The formation of α-Fe at the second TPR peak was confirmed by XRD. The XRD pattern for the sample after the second TPR peak is shown in Fig. 3c, which exhibits the characteristic diffraction peaks at $d = 2.03$ and 1.43 for α-Fe (31). Furthermore, the XRD pattern also showed the diffraction peaks for unreduced $Mg_{1-x}Fe_xO$ and MgO phase after the second TPR peak. The phases $Mg_{1-x}Fe_xO$ and MgO cannot be clearly resolved in the XRD pattern. The second TPR peak may correspond to the following reaction:

$$Mg_{1-x}Fe^{II}_xO + H_2 = \alpha\text{-Fe} + MgO + H_2O \qquad [4]$$

These results indicate that the reduction of Fe^{2+} to Fe is significantly retarded by the formation of solid solution $Mg_{1-x}Fe^{II}_xO$.

3. The Reduction Process of Mg–Fe–Al–O Trinary Oxide

Figures 4 and 5 show the Mössbauer spectra and XRD patterns, respectively, collected for the Mg–Fe–Al–O sample (Mg/Fe/Al = 2/1/1) before the TPR and after each TPR peak as represented in Fig. 1c. The Mössbauer parameters and assignments of corresponding iron species and the different phases detected by XRD are given in Table 2.

As shown in Fig. 4a, the sample before reduction displayed the Mössbauer spectrum with a sextuplet and a doublet in the center. The sextuplet has the inner hyperfine fields of 510 kOe and the isomer shift of 0.32 mm/s, characteristic of α-Fe_2O_3. The doublet with IS = 0.33 mm/s and QS = 0.76 mm/s can be attributed to $MgFeAlO_4$ following Putanov *et al.* (32). The linewidth of the sextuplet was substantially broadened, indicating the high dispersion of α-Fe_2O_3 throughout the sample. In addition, the peaks of the doublet were also broadened as compared to the corresponding doublet of Mg–Fe–O. This may be caused by the occurrence of a random distribution of constituent Fe^{3+} cations, owing to the presence of Mg^{2+} and Al^{3+} (33). The XRD pattern shown in Fig. 5a confirmed the existence of $MgFeAlO_4$ (34), α-Fe_2O_3 (35), and MgO (28).

The Mössbauer spectrum collected for the Mg–Fe–Al–O sample after the first TPR peak showed a sextuplet and two doublets in the center. The sextuplet has the inner hyperfine field of 327 kOe, characteristic of α-Fe. One doublet with IS = 0.14 mm/s and QS = 0.69 mm/s can be assigned to $MgFeAlO_4$ and the other with IS = 0.76 mm/s and QS = 1.10 mm/s may correspond to $Mg_{1-x}Fe_xO$. These species were confirmed by the XRD determination as presented in Fig. 5b. The disappearance of the sextuplet with the hyperfine field of 510 kOe in the Mössbauer spectrum revealed the reduction of α-Fe_2O_3. The reduction of α-Fe_2O_3 in Mg–Fe–Al–O might lead to the formation of $Mg_{1-x}Fe_xO$ and α-Fe. Table 2 shows that the spectral area of the $MgFeAlO_4$ was significantly decreased in the sample after the first TPR peak, indicating the reduction of this species at the first TPR peak. $MgFeAlO_4$ might also be reduced to $Mg_{1-x}Fe_xO$ and α-Fe. However, based on the previous argument that the presence of other cations such as

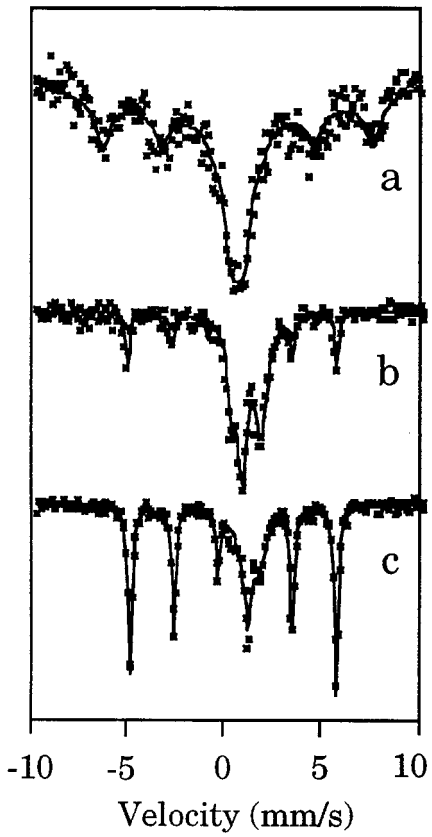

FIG. 4. *In situ* Mössbauer spectra for the Mg–Fe–Al–O sample with the Mg/Fe/Al ratio of 2/1/1 collected (a) before reduction, (b) after the first TPR peak, and (c) after the second TPR peak.

Mg^{2+} would retard the reduction of iron species, we suppose that α-Fe_2O_3 is easier to be reduced than $MgFeAlO_4$. Thus, the processes for the first TPR peak may be described as the reduction of α-Fe_2O_3 (with the presence of MgO) to α-Fe and $Mg_{1-x}Fe_xO$ and the reduction of part of $MgFeAlO_4$ to $Mg_{1-x}Fe_xO$. These processes may be expressed as follows:

$$\alpha\text{-}Fe_2O_3 + H_2 = \alpha\text{-}Fe + H_2O \quad [5]$$

$$\alpha\text{-}Fe_2O_3 + MgO + H_2 = Mg_{1-x}Fe^{II}_xO + H_2O \quad [6]$$

$$MgFe^{III}AlO_4 + H_2 = Mg_{1-x}Fe^{II}_xO + H_2O + Mg(Al)O. \quad [7]$$

It should be noted that the spinel species $MgAl_2O_4$ was not detected by XRD. The aluminum cations might be incorporated into the lattice of MgO, as described by McKenzie *et al.* (36). They expressed the phase as Mg(Al)O. Thus, we assume the same species formed during the reduction of $MgFe^{III}AlO_4$ as expressed by Eq. [7]. Another possibility is that aluminum cations may be incorporated into the $Mg_{1-x}Fe^{II}_xO$ phase. In fact, the $Mg_{1-x}Fe^{II}_xO$ phase for the Mg–Fe–Al–O sample after the reduction exhibited a much broader peak width and significantly larger QS in the Mössbauer spectrum. The presence of aluminum cations in the lattice of $Mg_{1-x}Fe^{II}_xO$ and the existence of the $MgFe^{III}AlO_4$ phase may be responsible for the much higher peak temperature of the second TPR peak for the Mg–Fe–Al–O sample.

The Mössbauer spectrum shown in Fig. 4c for the sample recorded after the second TPR peak is similar to the previous one except that the spectral areas for the species of $MgFeAlO_4$ and $Mg_{1-x}Fe_xO$ were significantly decreased

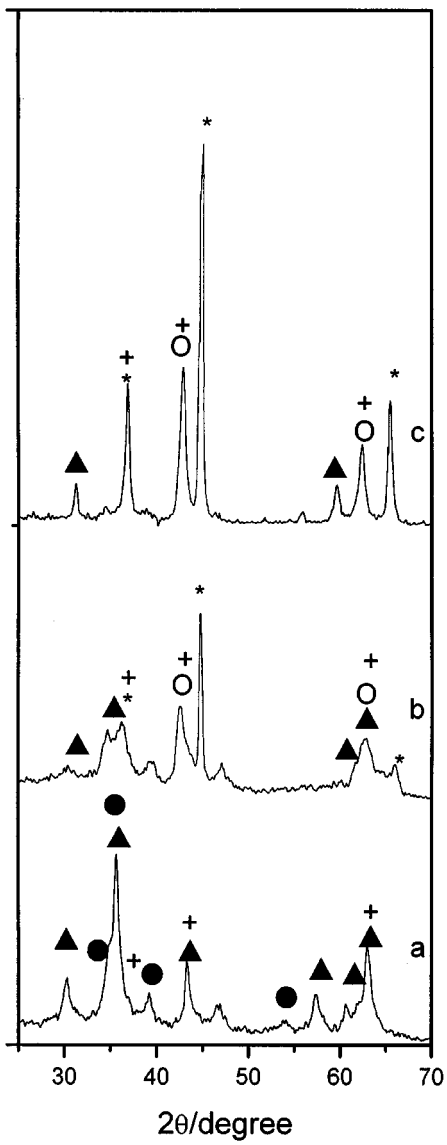

FIG. 5. The XRD patterns for the Mg–Fe–Al–O sample with the Mg/Fe/Al ratio of 2/1/1 collected (a) before the reduction, (b) after the first TPR peak, and (c) after the second TPR peak. The symbols for the phases are (●) Fe_2O_3, (▲) $MgFeAlO_4$, (+) MgO, (○) $Mg_{1-x}Fe_xO$, and (*) Fe.

TABLE 2
Mössbauer Parameters and Assignments of Iron Species and Phases Detected by XRD for the Fe–Mg–Al–O Sample (Mg/Fe = 2/1/1) before the Reduction and after Each TPR Peak

		Mössbauer results						
Peak in TPR	Peak temperature (°C)	IS ($mm\,s^{-1}$)	QS ($mm\,s^{-1}$)	HF (kOe)	FWHM ($mm\,s^{-1}$)	Relative peak area	Iron species assignment	Phases by XRD
Before reduction		0.32	—	510	—	43	α-Fe_2O_3	α-Fe_2O_3
		0.33	0.76	—	0.99	57	Fe^{3+}	$MgFeAlO_4$
								MgO
First peak	506	−0.14	—	333	—	19	Fe^0	Fe
		0.76	1.10	—	0.77	62	Fe^{2+}	$Mg_{1-x}Fe_xO$
		0.14	0.69	333	—	19	Fe^{3+}	$MgFeAlO_4$
								MgO
Second peak	936	0.01	—	327	—	69	Fe^0	Fe
		1.09	0.63	—	0.46	21	Fe^{2+}	$Mg_{1-x}Fe_xO$
		0.20	0.54	—	0.56	10	Fe^{3+}	$MgFeAlO_4$
								MgO

while the spectral area for α-Fe was greatly increased. The XRD pattern shown in Fig. 5c confirmed the existence of the phases $MgFeAlO_4$, $Mg_{1-x}Fe_xO$, and α-Fe. According to the Mössbauer data given in Table 2, it may be concluded that the processes for the second TPR peak of this sample involve the reactions

$$MgFe^{III}AlO_4 + H_2 = Mg_{1-x}Fe^{II}_xO + H_2O + Mg(Al)O \quad [7]$$

$$Mg_{1-x}Fe^{II}_xO + H_2 = \alpha\text{-}Fe + MgO + H_2O. \quad [8]$$

CONCLUSIONS

The reduction processes may reflect the interactions among various components in complex metal oxides. The technique of TPR combined with *in situ* Mössbauer spectroscopy is useful in understanding the reduction processes of iron-containing materials. The Mg–Fe–O binary oxides and Mg–Fe–Al–O trinary oxides may be prepared through the synthesis of hydrotalcite-like compounds. The reduction processes of these complex oxides were greatly affected by the formation of solid solutions. Specifically, the spinel $MgFe_2O_4$ in the Mg–Fe–O sample could be exclusively reduced to $Mg_{1-x}Fe_xO$, which was further reduced to α-Fe at the second TPR peak. In the Mg–Fe–Al–O sample, both α-Fe_2O_3 and $MgFeAlO_4$ are present before the reduction. At the first TPR peak, the α-Fe_2O_3 in the Mg–Fe–Al–O was converted to α-Fe and $Mg_{1-x}Fe_xO$ while the $MgFeAlO_4$ might only be converted to $Mg_{1-x}Fe_xO$. Hence, the reduction of iron species in the $MgFeAlO_4$ phase is further retarded by the presence of aluminum cations.

ACKNOWLEDGMENTS

This work is supported by the National Natural Science Foundation of China (Grant 29973013) and the Department of Science and Technology of China (Grant 1999022408). Financial support from the "333" project of Jiangsu Province is also acknowledged.

REFERENCES

1. M. Boudart, A. Delbouille, J. A. Dumesic, S. Khammouma, and H. Topsoe, *J. Catal.* **37,** 486 (1975).
2. R. Dutartre, P. Bussiere, J. A. Dalmon, and G. A. Martin, *J. Catal.* **59,** 382 (1979).
3. G. Poncelet, P. Grange, and P. A. Jacobs, *Stud. Surf. Sci. Catal.* (*Prep. Catal. III*) **16,** 385 (1983).
4. G. B. Raupp and W. N. Delgass, *J. Catal.* **58,** 337 (1979).
5. A. D. Logan and A. K. Datye, *J. Catal.* **112,** 595 (1988).
6. J. Shen, B. Guang, M. Tu, and Y Chen, *Catal. Today* **30,** 77 (1996).
7. W. S. Borghard and M. Boudart, *J. Catal.* **80,** 194 (1983).
8. M. A. McDonald, D. A. Storm, and M. Boudart, *J. Catal.* **102,** 386 (1986).
9. T. E. Holt, A. D. Logan, S. Chakrabarti, and A. K. Datye, *Appl. Catal.* **34,** 199 (1987).
10. P. Putanov, E. Kis, G. Boskovic, and K. Lazar, *Appl. Catal.* **73,** 17 (1991).
11. N. W. Hurst, S. J. Gentry, and A. Jones, *Catal. Rev.–Sci. Eng.* **24**(2), 233 (1982).
12. P. A. Barnes, G. M. B. Parkes, D. R. Brown, and E. L. Charsley, *Thermochim. Acta* **269/270,** 665 (1995).
13. P. A. Barnes, G. M. B. Parkes, and E. L. Charsley, *Anal. Chem.* **66,** 2226 (1994).
14. J. A. Dumesic and H. Topsoe, *Adv. Catal.* **26,** 121 (1977).
15. R. Tang, S. Zhang, C. Wang, D. Liang, and L. Lin, *J. Catal.* **106,** 440 (1987).
16. X. Ge, J. Shen, and H. Zhang, *Sci. China* (*Ser. B*) **39**(1), 53 (1996).
17. X. Ge, H. Zhang, and F. Wang, *Wuji Huaxue Xuebao* (*Chin. J. Inorg. Chem.*) **14**(3), 336 (1998).

18. X. Ge, Y. Wang, W. Zhang, J. Shen, and Q. Yuan, *J. Nanjing Univ.* (*Natural Sci.*) **35**(4), 511 (1999).
19. J. Jia, J. Shen, Z. Xu, X. Ge, T. Zhang, and L. Lin, *Gaodeng Xuexiao Huaxue Xuebao* (*Chin. J. Univ. Chem.*) **18**(6), 958 (1997).
20. X. Ge, Y. Wang, J. Shen, H. Zhang, *Wuji Huaxue Xuebao* (*Chin. J. Inorg. Chem.*) **16**(1), 79 (2000).
21. H. Zhang, J. Shen, and X. Ge, *J. Solid State Chem.* **117,** 127 (1995).
22. R. Tang, R. Wu, and L. Lin, *Appl. Catal.* **10,** 163 (1984).
23. A. J. H. M. Koch, H. M. Fortuin, and J. W. Geos, *J. Catal.* **96,** 261 (1985).
24. X. Gao, J. Shen, Y. Hsia, and Y. Chen, *J. Chem. Soc. Faraday Trans.* **89,** 1079 (1993).
25. R. G. Kulkarni and H. H. Joshi, *J. Solid State Chem.* **64,** 141 (1986).
26. G. Connell and J. A. Dumesic, *J. Catal.* **102,** 216 (1986).
27. JCPD Card 17-464. International Center for Diffraction Data, 1987.
28. JCPD Card 30-794. International Center for Diffraction Data, 1987.
29. M. Tu, J. Shen, and Y. Chen, *J. Solid State Chem.* **128,** 73 (1997).
30. Y. Qian, R. Kershaw, K. Dwight, and A. Wold, *Mater. Res. Bull.* **18,** 543 (1983).
31. JCPD Card 6-699. International Center for Diffraction Data, 1987.
32. P. Putanov, G. Boskovic, E. Kis, K. Lazar, and L. Guczi, *J. Solid State Chem.* **97,** 41 (1992).
33. H. Haneda, H. Yamamura, A. Watanabe, and S. Shirasaka, *J. Solid State Chem.* **68,** 273 (1987).
34. G. E. Bacon and A. J. E. Welch, *Acta Crystallogr.* **7,** 361 (1954).
35. JCPD Card 13-534. International Center for Diffraction Data, 1987.
36. A. L. McKenzie, C. T. Fishel, and R. J. Davis, *J. Catal.* **138,** 547 (1992).
37. L. Guczi, *Catal. Rev.–Sci. Eng.* **23,** 329 (1981).